PNAS RESEARCH ARTICLE | APPLIED PHYSICAL SCIENCES OPEN ACCESS

Observing the crack tip behavior at the nanoscale during fracture of ceramics

Oriol Gavalda-Diaz[a,b,1], Max Emmanuel[a], Andrey Berenov[a], Katharina Marquardt[a,c], Eduardo Saiz[a], and Finn Giuliani[a]

Edited by Anna Balazs, University of Pittsburgh, Pittsburgh, PA; received April 26, 2024; accepted September 11, 2024

Ultimately, brittle fracture involves breaking atomic bonds. However, we still lack a clear picture of what happens in the highly deformed region around a moving crack tip. Consequently, we still cannot link nanoscale phenomena with the macroscopic toughness of materials. The unsolved challenge is to observe the movement of the crack front at the nanoscale while extracting quantitative information. Here, we address this challenge by monitoring stable crack growth inside a transmission electron microscope. Our analysis demonstrates how phase transformation toughening, previously thought to be effective at the microscale and above, promotes crack deflection at the nanolevel and increases the fracture resistance. The work is a first step to help connecting the atomistic and continuous view of fracture in a way that can guide the design of the next generation of strong and tough materials demanded by technologies as diverse as healthcare, energy generation, or transport.

nanoscale | crack tip | fracture | TEM in situ testing | ceramics

Significance

To understand fracture and make brittle materials more ductile, we rely on modeling what happens at a crack tip. However, observing a crack tip in a brittle material is challenging: cracks propagate fast, and the events that we are interested in observing occur at the nanoscale or below. Up to now, we were not able to observe what happens ahead of a moving crack tip. In this work, we show how by carefully performing fracture experiments inside a transmission electron microscope we can grow stable cracks while observing the nanoscale events happening at the crack tip. This work will help linking continuous and atomistic models and support the design of the next generation of stiff, strong, and tough materials.

The structural capabilities of brittle materials such as ceramics or refractory metals are often limited by their poor fracture resistance. Not surprisingly, a large effort has been placed on increasing their toughness to meet the needs of a broad range of applications where their thermochemical resistance offers significant advantages (1–3). Multiple strategies have been implemented. They range from the transformation toughening exhibited by the zirconia ceramics used in orthopaedic implants (4) to crack bridging and fiber pull-out in ceramic matrix composites (CMCs) for nuclear and aerospace applications (5, 6). As the demands of the applications are continuously growing so does the need for even stronger and tougher materials (7). These developments have been accompanied by systematic studies on the fundamental mechanisms that determine fracture resistance and the ways to quantify it experimentally. However, and despite the maturity reached by the field, there is still a very significant gap between the well-established continuous linear-elastic analysis of toughness and the atomistic models of crack propagation. This gap limits our fundamental understanding and hampers practical progress.

The continuous linear elastic fracture mechanics (LEFM) analysis results in a stress singularity at the crack tip and goes around this issue by defining a "process zone" (with a typical size of few nanometers and below) around this tip where the behavior is no longer linear-elastic. It defines toughness as a critical stress concentration (K_c) that has to be reached for the crack to propagate. K_c determines the stress distribution away of the process zone at this critical point and can be linked to the fracture energy, G_c, through a very simple relationship ($G_c = K_c^2/E$, where E is the Young's modulus). Note that as reported by Issa et al. (8) plane stress conditions prevail in our tests as the sample thickness is similar in magnitude to the expected plastic zone (r_p) in a stiff and brittle ceramic. However, at the atomic scale, bond breaking at the crack tip happens within the process zone. According to the simplest of atomic views, the fracture energy should be equivalent to the one needed to create two new surfaces ($2\gamma_s$) but macroscopic experimental measurements are usually well above. This observation supports the accepted view that common toughening mechanisms in brittle materials act at the microscale by shielding the crack tip from the applied stresses and that some of these mechanisms could be detrimental to the strength of the material (2). Unfortunately, we still lack the comprehensive picture of how the fracture resistance develops from the atomic to the microscale and up. Furthermore, there is evidence suggesting that toughening may also occur at these scales and atomic models predict a series of phenomena such as lattice trapping (9), void formation ahead of the crack tip (10–12), or plasticity in the process zone (13) that are very challenging to verify experimentally. To support the rational design of the next generation of structural materials able to combine high strength and toughness, we need to address these open fundamental questions to build a holistic understanding of crack propagation and the generation of fracture resistance.

Author affiliations: [a]Department of Materials, Royal School of Mines, Imperial College London, London SW7 2AZ, United Kingdom; [b]Department of Mechanical, Materials and Manufacturing Engineering, Composites Research Group, Faculty of Engineering, University of Nottingham, Nottingham NG7 2GX, United Kingdom; and [c]Department of Materials, University of Oxford, Oxford OX1 3PH, Oxfordshire, United Kingdom

Author contributions: O.G.-D., E.S., and F.G. designed research; O.G.-D., M.E., and A.B. performed research; O.G.-D. and K.M. contributed new reagents/analytic tools; O.G.-D., K.M., E.S., and F.G. analyzed data; and O.G.-D., K.M., E.S., and F.G. wrote the paper.

The authors declare no competing interest.

This article is a PNAS Direct Submission.

Copyright © 2024 the Author(s). Published by PNAS. This open access article is distributed under Creative Commons Attribution-NonCommercial-NoDerivatives License 4.0 (CC BY-NC-ND).

[1]To whom correspondence may be addressed. Email: ogavalda@ic.ac.uk.

This article contains supporting information online at https://www.pnas.org/lookup/suppl/doi:10.1073/pnas.2408292121/-/DCSupplemental.

Published October 17, 2024.

Downloaded from https://www.pnas.org by "IMPERIAL COLLEGE LONDON, SUBSCRIPTIONS & E ACCESS" on October 22, 2024 from IP address 146.179.87.8.

In recent years, we have seen a very significant progress on the development of straining experiments from the micron to the nanoscale coupled with in situ high-resolution imaging (14). This includes the development of new TEM in situ setups capable of linking the performance of materials to atomic and nanoscale events such as the role of interfaces in plastic deformation (15) or the effect of ion intercalation in energy storage devices (16). These setups create new opportunities to observe the materials response close to a crack tip. The results show that while in some materials the fracture energy at the microlevel approaches the expected theoretical value of twice the surface energy (once extrinsic toughening mechanisms acting at larger length scales are eliminated) (17), in others, this is not the case (18, 19). In this respect, in situ nanomechanical testing in the transmission electron microscope (TEM) offers the possibility to observe crack propagation at the nanoscale and get closer to those accessible in atomistic simulations. Further developments in this direction should enable us to link directly model and observation and obtain quantitative data that combined with experiments at larger length scales can feed the much-needed comprehensive multiscale failure models. Several in situ nanomechanical testing setups in the TEM have been developed with the aim of observing and quantifying the plastic deformation that brittle materials experience at the nanoscale by either using tension (20–24), shear (23), and compression (23, 25, 26) setups. Fracture indentation (27–29) and single cantilever bending (30) tests have also been used to propagate cracks and evaluate their fracture morphology at this scale. Nevertheless, in these setups, cracks in brittle materials propagate in an unstable manner. Therefore, it is possible to observe the material immediately before and immediately after fracture, but the information that can be extracted of the nanoscale events occurring during the progression of a crack front is very limited. To address this challenge, we are proposing an approach capable of recording nanoscale dynamic events during crack propagation.

Being inspired by the original work from Obreimoff (31) and the later adaption of the test to SEM (17) and TEM (32) in situ setups, we are proposing an optimized wedge-driven double cantilever beam (DCB) test which achieves stable crack growth inside a TEM when testing stiff and brittle materials. This setup helps us to enhance our mechanistic understanding of failure by resolving in situ the nanoscale structure of the crack front during propagation. We use this technique to study the fracture of two model brittle materials, SiC, the base of modern tough CMCs, and ZrO_2, the poster material for transformation toughening used now in high-end applications such as orthopaedic implants or thermal barrier coatings. In the later material, our in situ setup enables something that has been considered "impossible or really difficult" (33): resolving the transformation toughening at the crack tip. Our work shows how stress shielding happens during early stages of crack propagation and reports the toughening mechanisms active at the single grain level. Our observations show how a stress-activated phase transformation occurs well below the microscale, challenging the rules of brittle crack growth.

1. Results

1.1. In Situ Stable Crack Growth at the Nanoscale. We use a TEM in situ setup to visualize the nanoscale events occurring when cracks propagate in brittle materials. The notable feature of this setup is that we can achieve stable crack growth even when testing brittle and stiff materials such as SiC or ZrO_2. The stable nature of the crack allows us to use the wide range of analytical techniques available in a TEM to describe the nanoscale structure around a crack tip. This has been achieved by redesigning the wedge-driven DCB test traditionally used to measure fracture properties of materials at the macroscale and more recently implemented in SEM and TEM in situ tests (17, 32). In our setup, we propose a method which uses relatively large samples (approx. 2 × 2 × 0.1 mm) and in which nano-DCB samples are prepared using focused ion beam (FIB). The DCBs contain two thick arms (approx. 1 × 1 μm) to facilitate the position of the wedge and reduce the through-thickness compliance. An electron transparent region (approx. 1 × 0.1 μm) is milled at the center to observe the fracture process at the nanoscale (Fig. 1). The opening displacement of the arms is applied with a custom-built diamond wedge with an angle of ≈ 65°. Overall, the reduced compliance of the setup allows us to stabilize the fracture test and to resolve the fracture process at the nanoscale (*SI Appendix*, Fig. S2). We can also pause the test at a given opening displacement and analyze the crack tip with the analytical techniques available in the TEM. More details on the sample preparation and testing conditions are given in *SI Appendix*, *Methods*. In this work, we show an example of how we combine TEM imaging and diffraction to explain the fracture process of SiC and ZrO_2-based materials.

1.2. Crack Tip Behavior during Brittle Fracture. Our stable crack growth experiments allow us to observe how a crack tip moves within a "model" brittle ceramic material such as hexagonal SiC (6H-SiC). Fig. 2*A* shows a frame obtained during the stable crack propagation experiment splitting the basal plane (see also *SI Appendix*, Fig. S3 and Movie S1). By using the TEM micrograph frames obtained during the in situ experiment, we get the near crack tip profile by measuring the crack opening (2u) at different distances from the crack tip (x). Based on Irwin's equation we can link the near tip profile to the toughness of the material by using Eq. **1** (34, 35).

$$u(x) = \frac{K_{ic}}{E}\sqrt{\frac{8x}{\pi}}. \quad [1]$$

In this case, we are simplifying the analysis by not taking into consideration the anisotropy of the crystal and considering a Young's modulus of E_{SiC} = 480 GPa. We use two values of toughness K_{Ic} = 3.3 and 2.18 $MPa.m^{1/2}$ which represent the literature data available for SiC at the macroscale and twice the surface energy obtained with DFT simulations [17], we plot Eq. **1** together with our experimental values (Fig. 2*B*). The error analysis coming from the measurement of the crack opening from the TEM frames has been taken into consideration in the experimental data points and has been detailed in *SI Appendix*, Figs. S4 and S5. Our nanoscale fracture data are in good agreement with the fracture toughness found at the micron scale and suggest that the fracture energy values (i.e., toughness) are close to the twice surface energy ($2\gamma_s$) of the material (17) as expected from an ideal brittle fracture.

As early suggested by Irwin, LEFM builds on the assumption that in brittle materials, a small process zone forms ahead of the crack tip. This is needed to address the stress singularity generated at this tip by the continuous analysis. The different theories agree that when the process zone is generated by plasticity, its extension depends on the toughness (K_{Ic}) and yield stress (σ_y) of the material. In general, it is well established that the size is proportional to $(K_{Ic}/\sigma_y)^2$ and in ceramics is expected to be of the order of nanometers.

Our test allows us to monitor the nanoscale events happening at the crack tip when fracturing SiC. Differently from a postmortem analysis, this is done while the wedge is inserted with the arms bent. Therefore, we can observe the zone around the crack tip in situ while the load is applied. Fig. 2*C* shows the crack tip behavior when growing a crack for ≈ 40 nm along the basal plane. There is a damaged area ahead of the tip (of size 30 to 50 nm) which resembles the

Downloaded from https://www.pnas.org by "IMPERIAL COLLEGE LONDON, SUBSCRIPTIONS & E ACCESS" on October 22, 2024 from IP address 146.179.87.8.

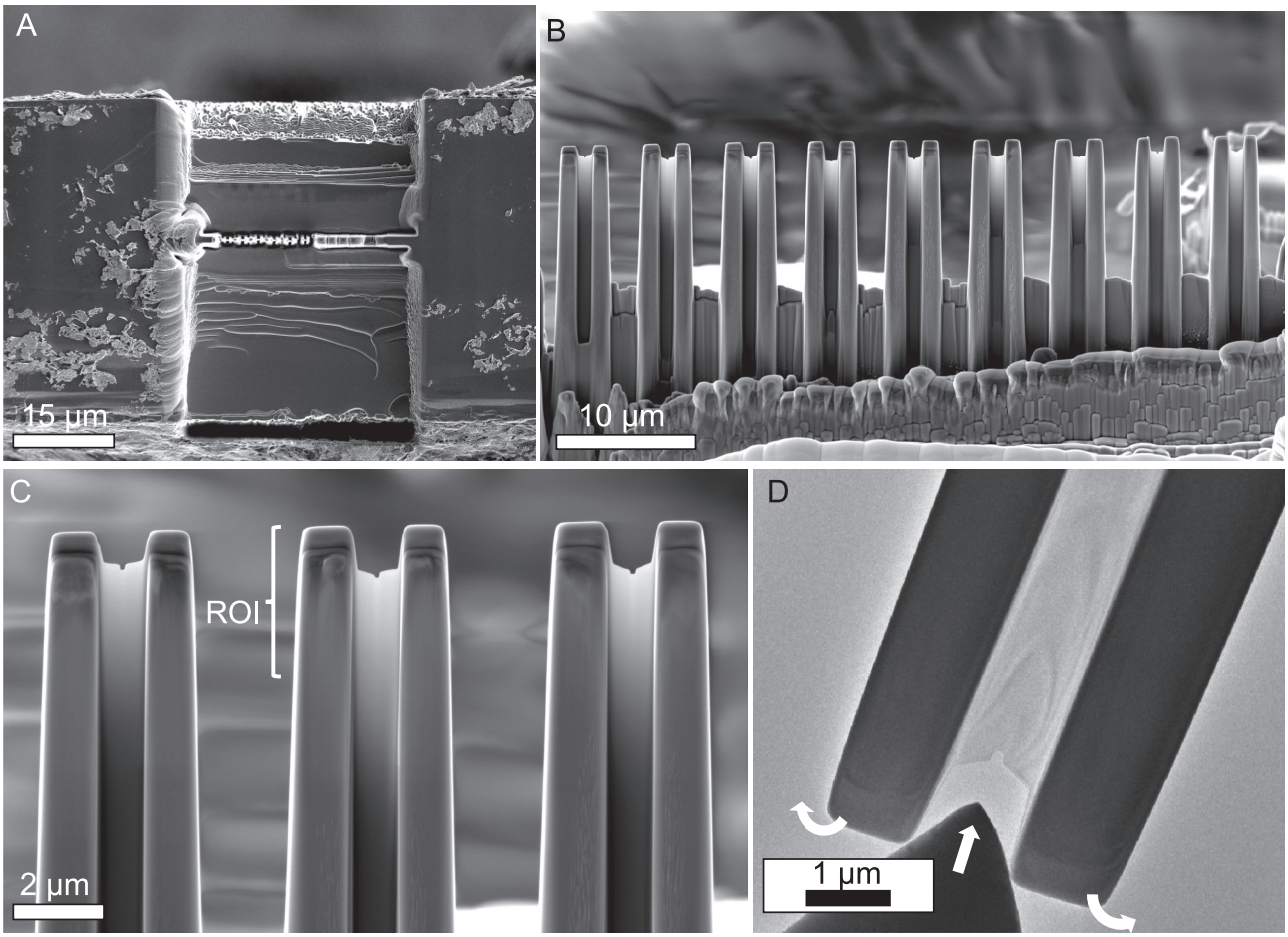


Fig. 1. Nanofabricated single-crystal DCBs. (*A*) Top view of the sample after being thinned. (*B*) Front view of several DCBs. (*C*) Close-up of a DCB showing the two arms (approx. cross section of 1 × 1 μm) and the thinned region (approx. 1 × 0.1 μm) with a FIB-milled notch. The region of interest (ROI) shows the length of the sample used for crack growth (≈1 to 2 μm). (*D*) Wedge-actuated DCB test showing early stages of the loading and the bending contours around the notch.

process zone shape expected for a Mode I fracture test (36). Based on our fracture toughness data we use, a value of K_I = 2.18 MPa. $m^{1/2}$ to plot in Fig. 2*D* the theoretical process zone overlapped with our experiments (*SI Appendix*, Eq. **S1**) for three arbitrary values of stress (5, 10, and 15 GPa) that give either good correlation with our experimental data or with the expected yield stress. The stress values can be seen as a cut off value helping to visualize the extension of the process and plastic zones. In SiC, a plastic zone with a radius between 30 and 50 nm suggests a yield stress of around 5 GPa. Literature in 6H-SiC reports a critical resolved shear stress (τ_{CRSS}) for basal and prism slip (<a> type) of 5 to 6 GPa (37). Because we are propagating a crack along the basal plane, the main slip system available is <a+c> type, which is tilted ≈ 83° from <a> (our crack propagation direction (see *Inset* in Fig. 2 *C*, i). Hence, we should assume that the minimum yield stress will be $\sigma_y \approx 2\tau_{CRSS} \approx 10$ to 12 GPa, as <a> is generally a softer plane than <a+c> (38). A yield stress of >10 GPa will result in a plastic zone smaller than 10 nm and hence smaller than the process zone identified using the grayscale in the in situ TEM image. This suggest that what we observe at the crack tip is a combination of a plastic zone surrounded by an area of high elastic strain. These observations highlight the complex mechanisms of cohesive zone formation. Further work looking at characterizing the strain in the process region should be explored in the future.

1.3. Toughening of Ceramics At the Nanoscale. To observe toughening at the nanoscale, we select ZrO_2 due its exceptional capability for the customization of fracture resistance. This is achieved by stabilizing the tetragonal phase at room temperature using low contents of an oxide, commonly yttria or ceria. The tetragonal phase transforms to monoclinic in the presence of stress, for example, at the crack tip. This transformation is diffusionless and of martensitic nature and induces compressive residual stresses ahead of the crack and can result in a three- or fourfold increase in fracture toughness at the macroscale (39, 40). In the case of yttria-stabilized zirconia (YSZ), low contents of yttria (3 to 8 mol%) can stabilize the tetragonal phase with a high toughness. When stabilizing the cubic phase (8 to 12 mol%), the toughness increase is lost. In this work, we test single crystal regions of yttria stabilized zirconia with 4 and 9.5 mol% (4YSZ and 9YSZ) to follow the nanoscale response of the tetragonal and cubic polymorphs, respectively.

DCB tests were performed splitting ≈(001) planes in both samples. In the case of 9YSZ, straight cracks (with an absence of deflection and twisting) are systematically observed and highlight the brittle nature of the material (Fig. 3*A* and Movie S2). High-resolution TEM images and diffraction studies confirm the lack of phase transformation and a plastic zone of around 10 nm (Fig. 3*B*).

When testing 4YSZ, we observe how cracks follow a more tortuous path with evidence of crack deflection and twisting (Fig. 3*C* and Movie S3). Similar crack growth mechanisms were observed in all the tests (*SI Appendix*, Fig. S6). This suggests that the crack is being redirected by the local nanostructure formed ahead of the tip. It is remarkable to observe how deflection and twisting mechanisms, common in bulk fracture testing of polycrystals yttria-stabilized zirconia (40), arise at the nanometer scale within a single grain.

Downloaded from https://www.pnas.org by "IMPERIAL COLLEGE LONDON, SUBSCRIPTIONS & E ACCESS" on October 22, 2024 from IP address 146.179.87.8.

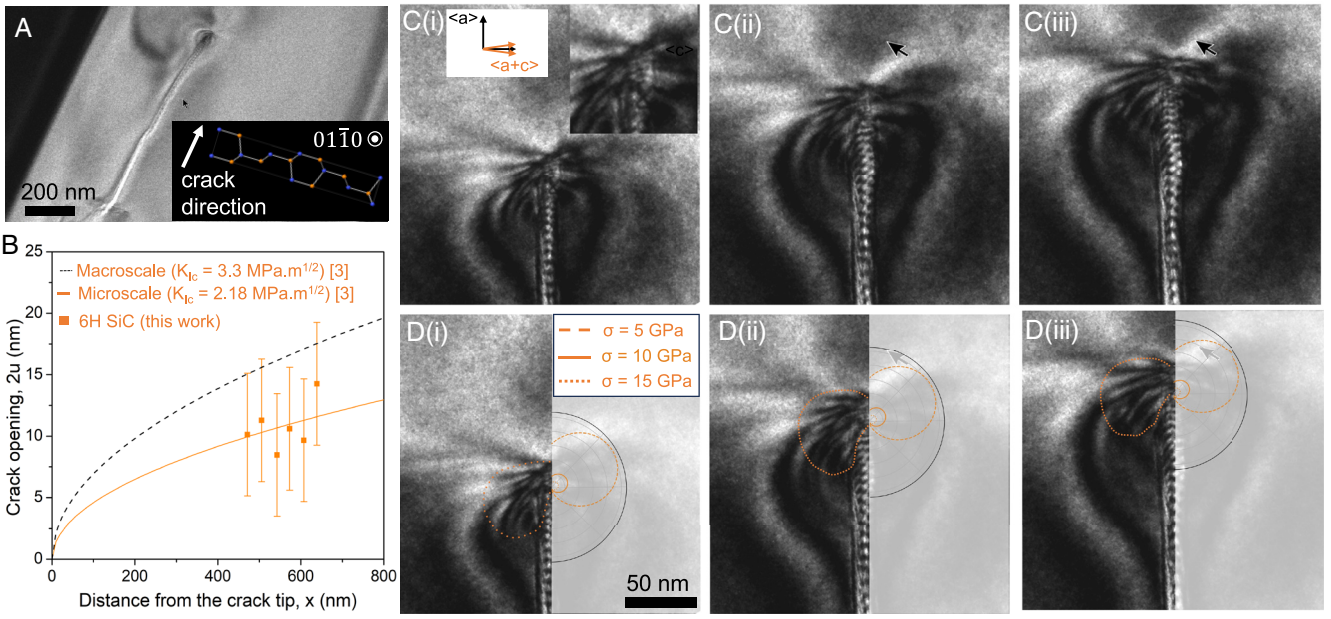


Fig. 2. Stable crack growth in SiC. (*A*) Lower magnification images of the crack. (*B*) Crack openings (2u) at different distances from the crack tip overlapped with the expected values of toughness at the micron and macroscales. (*C*) High-magnification frames showing the progress of the crack tip (Movie S1), *Insets* in (i) show the approximate direction of <a+c> with respect to the crack direction and a higher magnification image of the crack tip. (*D*) Frames overlapped with the predicted plastic zone for different values of yield stress (σ_y). The contour used to highlight the experimental process zone is just an approximation to guide the eye of the reader.

By following the same approach as with SiC, we use the crack opening to measure the toughness of ZrO_2 at the nanoscale (Fig. 4*A*). Considering a Young modulus of E_{4YSZ} = 214 GPa and E_{9YSZ} = 220 GPa (41) [similar to the ones reported in micromechanical testing (42)], our data suggest approximate values of nanoscale fracture toughness of 1.8 and 2.7 MPa.m$^{1/2}$ for 9YSZ and 4YSZ, respectively, for crack lengths shorter than 1 μm. Note that for the 4YSZ samples, we analyze cracks with minimal deflection to ensure an accurate measurement of the crack tip distance (x). This also highlights that the increase in toughness reported here is mainly dictated by the phase transformation and not due to an increase of crack surface.

Fig. 4*B* compares the values of fracture toughness that we measure for single crystals at the nanoscale with average literature data for polycrystalline YSZ tested at the macroscale (39) and microscale data available for nanocrystalline 3YSZ (43). 9YSZ shows good agreement with the values measured in macroscopic cubic polycrystalline YSZ samples, highlighting its brittle nature and absence of active extrinsic toughening mechanisms in the material, hence $G_c^{9YSZ} \approx 2\gamma_s$. In the case of 4YSZ, we measure lower values compared to the reported ones for large tetragonal zirconia polycrystalline (TZP) samples but around 50% larger than for 9YSZ. Assuming that the surface energy for the (001) in cubic and tetragonal YSZ crystals is similar and the fracture energy of tetragonal zirconia can be expressed as $G_c^{4YSZ} = 2\gamma_s + G_{transf}$ (with G_{tranf} being the contribution due to phase transformation), we can conclude that phase transformation contributes ≈ 50% to the overall fracture energy measured.

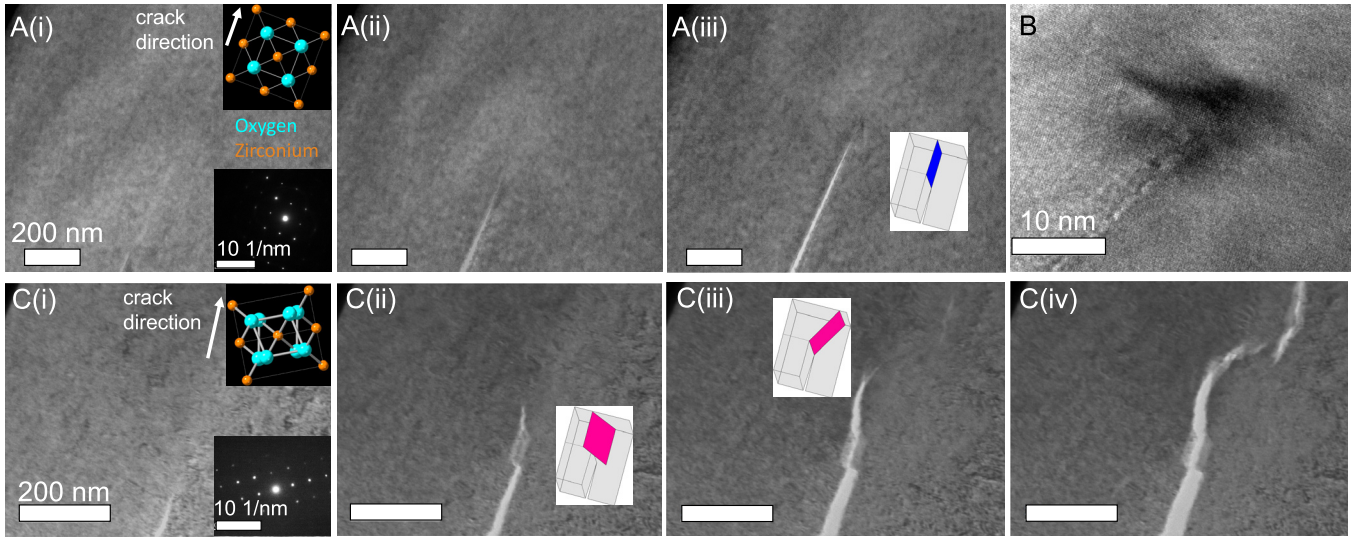


Fig. 3. Stable crack growth in ZrO_2. (*A*) Splitting the ≈(001) plane in the cubic polymorph (9YSZ) and showing how the crack propagates straight without deflection/twisting (Movie S2). (*B*) High-magnification image of the crack tip in 9YSZ, showing the lack of phase transformation. (*C*) Splitting the ≈(001) plane in the tetragonal polymorph (4YSZ) highlighting the crack tilting and twisting (Movie S3).

Downloaded from https://www.pnas.org by "IMPERIAL COLLEGE LONDON, SUBSCRIPTIONS & E ACCESS" on October 22, 2024 from IP address 146.179.87.8.

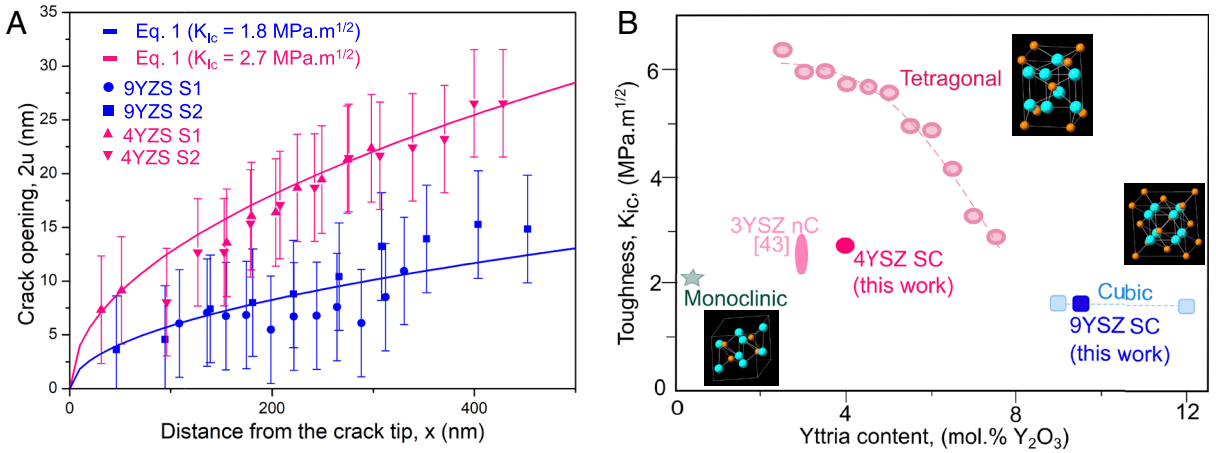


Fig. 4. Fracture toughness of zirconia at the nanoscale. (*A*) Crack openings (2u) at different distances from the crack tip (x) for 4YSZ and 9YSZ and the calculated K_{IC} obtained by fitting Eq. **1**. (*B*) Average literature toughness values for the different polymorphs of polycrystalline YSZ at the macroscale (data extracted from ref. 39) overlapped with microscale data for nanocrystalline (nC) 3YSZ (data extracted from ref. 43) and our data of toughness at the nanoscale.

The difference between our nanoscale experiment and the macroscale data highlights how the transformation zone and crack shielding can be dependent on the following factors:

(i) Length scale: When tested at the macroscale in vacuum, TZP displays a rising R-curve (44), suggesting that the transformation zone ahead of the crack tip increases with crack length. Similar values of toughness (2.0 to 2.5 MPa.m$^{1/2}$) are obtained when testing nanocrystalline tetragonal 3YSZ at the micron scale (propagating a crack for 1 to 3 microns) (43). Typically, the postmortem analyses of macroscopic samples show fully transformed grains around the crack. Our data shows how toughening starts at very short crack lengths and how the toughening mechanisms are activated within a single grain with a transformation zone that forms and increases in size after the crack propagates for few nanometers.

(ii) Sample geometry: In our work, we propagate cracks within an electron transparent region, removing part of the 3D nature of the transformation zone and also limiting the coincidence planes in which tetragonal to monoclinic phases can nucleate.

(iii) Microstructure: Within a polycrystalline material, random grain orientations might produce transformation zones with more complex residual stress fields and more tortuous crack paths.

Because our data agree with the toughness values reported at the microscale, we believe that from the 3 factors proposed, length scale might be the dominant one.

Overall, with our work, we highlight that the toughening mechanisms traditionally reported in zirconia can already be active in early stages of crack propagation and within a single grain. By doing the experiment inside a TEM, we can also explore the nanoscale events dominating this toughening mechanism.

1.4. Transformation Toughening at the Crack Tip. The transformation toughening leading to the tortuous crack path in tetragonal zirconia is studied more in depth by performing tests at higher magnifications and highlighting diffraction contrast with a smaller objective aperture in the TEM. When the crack tip advances, we observe how darker regions form ahead of the crack tip (Fig. 5*A*). These darker regions nucleate in the crack front and suggest that a stress-activated tetragonal to monoclinic phase transformation is progressing (Movie S4).

Fig. 5*B* shows the crack in Fig. 5*A* after being fully unloaded and reloaded (Movie S5). See the load–displacement curve for the first and second loading in Fig. 5*C*. When the load is removed, the dark areas remain present in the sample indicating a stable and permanent nature (Fig. 5 *B*, i). During the regrowth of the crack (Fig. 5 *B*, ii–v), the extent of the darker areas continue to spread ahead of the crack tip. The shape of the darker area resembles the transformation zone predicted under dilatation and shear stresses in Mode I (40). Lower magnification images of the extent of the darker regions at different stages of loading and unloading are also shown in *SI Appendix*, Fig. S7.

The nature of the transformation zone is studied via diffraction and high-resolution imaging. Extra spots in the diffraction pattern (see *Inset* in Fig. 5*F*) confirm the presence of the monoclinic phase after crack propagation. The possible monoclinic orientations matching the diffraction patters appears to suffer from a ≈45° rotation from expected lattice correspondence (*SI Appendix*, Fig. S8) (45). This is attributed to surface relief caused by the volume expansion in our electron transparent samples.

To qualitatively assess the extent of the transformation process we use selected area diffraction (SAD). We measure diffraction spots corresponding to the monoclinic phase up to ≈ 500 nm away from one the side of the crack, but their intensity decreases when moving further away (Fig. 5 *I*, i and ii). At a distance of 300 nm ahead of the crack tip and in the other side of the crack, there is no evidence of phase transformation (Fig. 5 *I*, iii and iv). *SI Appendix*, Fig. S9 shows a higher magnification analysis of the lateral extent of the phase transformation. The data suggest that the transformation nucleating at the crack tip (≈100 nm) grows in the crack wake during the bending of the beams. Our data also show the subcritical nature of phase transformation in which remaining tetragonal phase is observed in the transformed regions and imply the coexistence of the monoclinic and tetragonal phases.

Higher magnification TEM images at the vicinity of the crack (Fig. 5 *G* and *H*) show Moiré fringes which suggest that the monoclinic phase nucleates as twins forming a herringbone structure with monolithic laths within a tetragonal matrix (46). This is further confirmed by the long streaks observed in the diffraction pattern (*Inset* in Fig. 5*F*) and which confirm the 2D nature of the defects. Dark field (DF) TEM images of the crack path isolating different monoclinic diffraction spots also confirm the presence of the monoclinic phase especially where the Moiré fringes are observed (*SI Appendix*, Fig. S10).

Downloaded from https://www.pnas.org by "IMPERIAL COLLEGE LONDON, SUBSCRIPTIONS & E ACCESS" on October 22, 2024 from IP address 146.179.87.8.

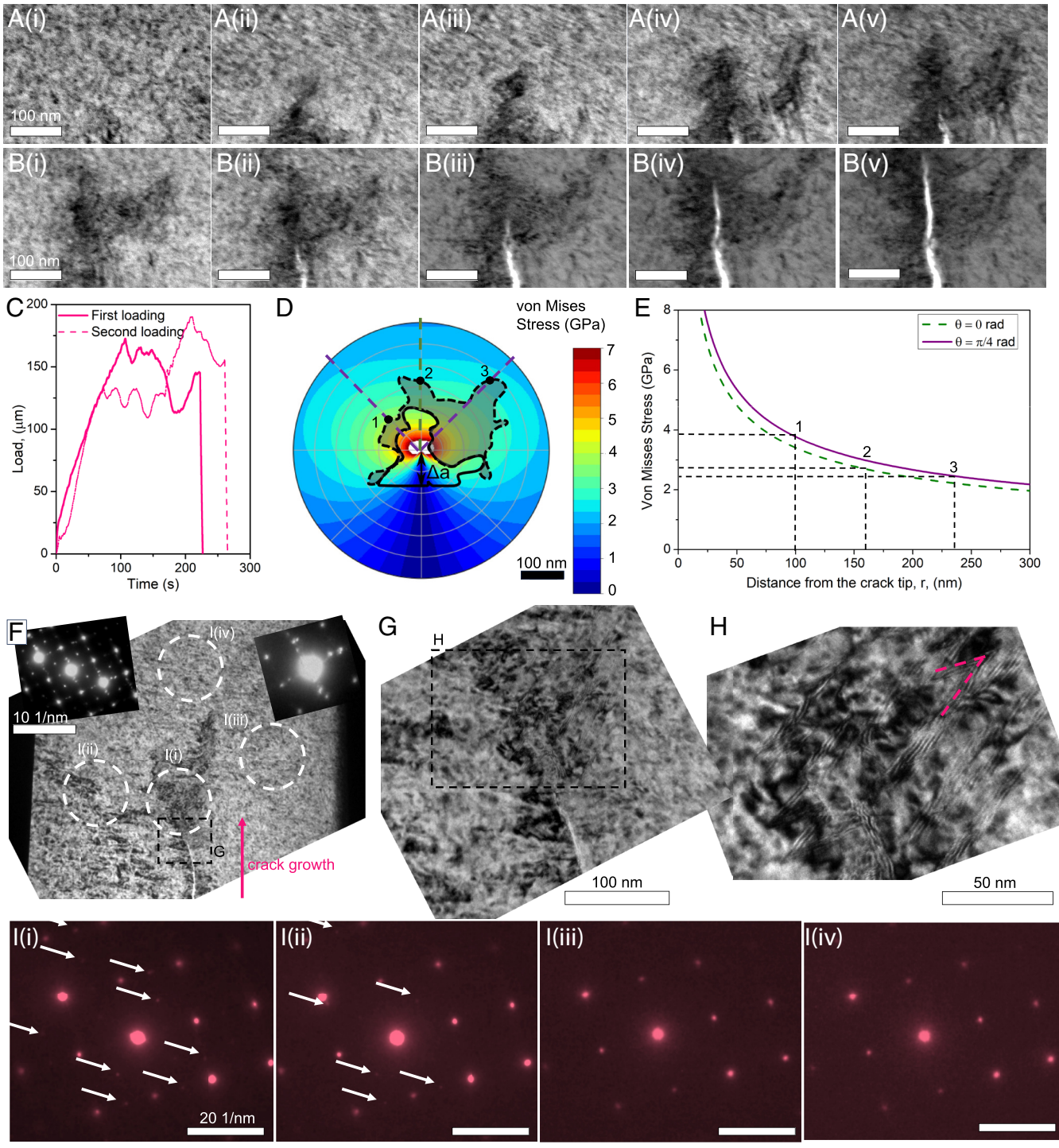


Fig. 5. Transformation toughening in tetragonal zirconia. (*A*) Darker regions forming ahead the crack tip (Movie S4). (*B*) Regrowth of the crack in A after the sample was unloaded and showing how the darker regions keep nucleating and growing ahead of the crack tip (Movie S5). (*C*) Load–time curves for the loading and reloading test in *A* and *B*. (*D*) Growth of the transformation zone overlapped with the Von Mises stresses with profiles for θ = 0 and 45° in (*E*). (*F*) Low magnification image of the overview of the crack and the four regions used for the SAD measurements. The *Insets* are the DP of the sample after testing. (*G* and *H*) Higher-magnification images of the crack showing the formation of moiré fringes and suggesting the formation of a herringbone structure. (*I*) SAD patterns with arrows highlighting the diffraction spots corresponding to the monoclinic phase.

We use the TEM frames to quantify the extent of the transformation zone around the crack tip. The shaded area in Fig. 5*D* shows an example of the growth of transformation zone for an increase of crack length (Δa) of ≈75 nm (see *SI Appendix*, Fig. S11). The growth in transformation zone is overlapped with the von Mises stresses predicted via LEFM (*SI Appendix*, Fig. S12) when propagating a crack in Mode I and using as stress intensity factor K_I = 2.7 MPa.m$^{1/2}$. To help visualize the stresses reached at the edge of the transformation zone, we plot 2D stress profiles for two given θ angles: 0 and 45° (see green and purple lines in Fig. 5*E*). Our results suggest that the critical stress required to trigger the tetragonal to monoclinic phase transformation oscillates between 2 and 4 GPa. These results agree with the yield stress reported for 3YSZ when testing at the microscale using pillar compression (42).

Downloaded from https://www.pnas.org by "IMPERIAL COLLEGE LONDON, SUBSCRIPTIONS & E ACCESS" on October 22, 2024 from IP address 146.179.87.8.

2. Conclusions

In this study, we have measured the toughness at the nanoscale while observing in situ the nanoscale structure ahead of an advancing crack front in different ceramics. By combining different imaging and diffraction techniques, we can explain how this nanostructure is affected by the extreme stress field generated by the crack and how this influences the fracture properties of the material at the nanoscale. We have first shown the progress of the damaged zone ahead of the crack tip when testing model brittle materials such as hexagonal SiC or cubic ZrO_2 (9YSZ). Our data suggest that this process zone is of the order of a few nm. The measured toughness approaches the ideal value of twice the surface energy that could be expected in the small-scale experiments when there is no contribution from large-scale extrinsic toughening mechanisms. From this baseline, we expand our analysis to study the failure process in the presence of transformation toughening in tetragonal ZrO_2 (4YSZ). We have shown how we can resolve the stress-induced phase transformation operating ahead of a crack tip and reveal its nanostructure during crack growth. This has given us unprecedented information on how phase transformation changes the local nanostructure and the critical stress required to activate it. Phase transformation at the nanoscale promotes crack deflection within a single grain and contributes the fracture resistance for cracks that are only hundreds of nanometers in length.

Overall, this work has shown how visualizing the advance of a crack in situ at the nanoscale could help to unveil the processes active at the tip during propagation while measuring fracture properties at the nanoscale. The goal is to bring the experimental length scales a bit closer to these that can be directly implemented in atomistic models in way that will help us understand how fracture resistance operates at different length scales. This work uses only a small fraction of the possible techniques available in a TEM and other techniques, including spectroscopy or 4D STEM (8), could be explored in order to learn more about the coupling of structure and chemistry during fracture. The final goal should be to enhance our fundamental understanding of fracture, linking continuous and atomistic models in a way that will support the design of the next generation of stiff, strong, and tough materials.

3. Methods

3.1. Materials. Three ceramics were used for this study: i) single crystals of 6H-SiC oriented along the (0001) supplied by MTI Corporation, ii) single crystals of ZrO_2 9.5% Y_2O_3 (9YSZ) oriented along the (100) direction supplied by Princeton Scientific Corporation, and iii) single crystals of ZrO_2 4% Y_2O_3 (4YSZ) oriented along the (001) direction supplied by Pi-Kem. The 4YSZ crystals measured 3 × 3 × 0.5 mm and were produced using the skull melting process. Characterization of the as-received crystals showing its tetragonal nature has been shown in *SI Appendix*, Fig. S1.

3.2. Sample Preparation. Both materials were polished down to 50 to 200 μm thickness using diamond suspensions (6, 3, and 1 μm successively). Afterward, the samples were placed with the thin edge facing up and the thickness was further reduced locally using a SEM/FIB station (Helios Dual Beam, FEI, US), as shown in Fig. 1*A*. The currents used were reduced from 9 nA to 1 nA and finishing at 0.3 nA, all at 30 kV.

Once the thickness of the sample was reduced to around 3 μm, DCBs were milled with the FIB using 30 kV and 0.3 nA. The center of the DCB (electron transparent region of around 1 μm in width) was finished at 30 kV and 20 pA. A notch was milled using the same conditions used in the last step. A final cleaning was performed at 5 kV and 20 pA, until the top of the thin area was around 50 to 100 nm (Fig. 1*C*). EELS was used to confirm the thickness range of the samples.

3.3. Tip Preparation. A Berkovich indenter commercially available from Hysitron to be used in the TEM in situ holder was modified to a wedge with the FIB. First, the bottom of the tip was flattened by removing the edge of the Berkovich at 6 nA. Afterward, the wedge shape was created by placing the tip perpendicular to the ion beam and tilting the tip ± 30°. The final tip geometry had an angle of ≈ 65° and can be seen in Fig. 1*D* and *SI Appendix*, Fig. S2*B*.

3.4. Nanomechanical Testing. Fracture tests were performed with a HysitronTM PI 95 TEM PicoIndenter holder, a TEM in situ mechanical holder. The tests were performed in a FEG TEM (2100F, JEOL, Japan) operating at 200 kV. The displacement rate of the wedge was 1 nm/s, the minimum allowed by the holder to ensure a stable crack propagation. The test was stopped when the crack propagated outside the field of view. Cracks were propagated within the first 1 to 2 μm. The tests were performed at different magnifications to provide an understanding of how crack propagate from the micron to the nanometer scales.

Data, Materials, and Software Availability. All study data are included in the article and/or supporting information.

ACKNOWLEDGMENTS. We would like to thank the Engineering & Physical Sciences Research Council Future Manufacturing Hub in Manufacture using Advanced Powder Processes, EP/P006566/1.

1. A. G. Evans, Perspective on the development of high toughness ceramics. *J. Am. Ceram. Soc.* **73**, 187–206 (1990).
2. R. O. Ritchie, The conflicts between strength and toughness. *Nat. Mater.* **10**, 817–822 (2011).
3. R. O. Ritchie, Toughening materials: Enhancing resistance to fracture. *Philos. Trans. R Soc. A: Math., Phys. Eng. Sci.* **379**, 20200437 (2021).
4. J. Chevalier *et al.*, Forty years after the promise of "ceramic steel?": Zirconia-based composites with a metal-like mechanical behavior. *J. Am. Ceram. Soc.* **103**, 1482–1513 (2020).
5. P. Baldus, M. Jansen, D. Sporn, Ceramic fibers for matrix composites in high-temperature engine applications. *Science* **285**, 699–703 (1999).
6. D. B. Marshall, B. N. Cox, Integral textile ceramic structures. *Annu. Rev. Mater. Res.* **38**, 425–443 (2008).
7. S. E. Prameela *et al.*, Materials for extreme environments. *Nat. Rev. Mater.* **9**, 6 (2022).
8. I. Issa *et al.*, In-situ TEM investigation of toughening in silicon at small scales. *Mater. Today* **48**, 29–37 (2021).
9. R. Thomson, C. Hsieh, V. Rana, Lattice trapping of fracture cracks. *J. Appl. Phys.* **42**, 3154–3160 (1971).
10. F. Célarié *et al.*, Glass breaks like metal, but at the nanometer scale. *Phys. Rev. Lett.* **90**, 4 (2003).
11. L. Q. Shen *et al.*, Observation of cavitation governing fracture in glasses. *Sci. Adv.* **7**, eabf7293 (2021).
12. K. I. Nomura *et al.*, Interaction and coalescence of nanovoids and dynamic fracture in silica glass: Multimillion-to-billion atom molecular dynamics simulations. *J. Phys. D Appl. Phys.* **42**, 214011 (2009).
13. E. Bitzek, J. R. Kermode, P. Gumbsch, Atomistic aspects of fracture. *Int. J. Fract.* **191**, 13–30 (2015).
14. G. Dehm, B. N. Jaya, R. Raghavan, C. Kirchlechner, Overview on micro- and nanomechanical testing: New insights in interface plasticity and fracture at small length scales. *Acta Mater.* **142**, 248–282 (2018).
15. Z. Shan *et al.*, Grain boundary-mediated plasticity in nanocrystalline nickel. *Science* **305**, 654–657 (2004).
16. X. H. Liu, Y. Liu, A. Kushima, S. Zhang, T. Zhu, In situ TEM experiments of electrochemical lithiation and delithiation of individual nanostructures. *Adv. Energy Mater.* **2**, 722–741 (2012), 10.1002/aenm.201200024.
17. G. Sernicola *et al.*, In situ stable crack growth at the micron scale. *Nat. Commun.* **8**, 108 (2017).
18. O. Gavalda-Diaz *et al.*, Basal plane delamination energy measurement in a Ti_3SiC_2 MAX phase. *JOM* **73**, 1582–1588 (2021).
19. N. Aldegaither *et al.*, Fracture toughness of bone at the microscale. *Acta Biomater.* **121**, 475–483 (2021).
20. C. Dang *et al.*, Achieving large uniform tensile elasticity in microfabricated diamond. *Science* **78**, 76–78 (2021).
21. P. Li *et al.*, In situ observation of fracture along twin boundaries in boron carbide. *Adv. Mater.* **35**, 2204375 (2022).
22. T. C. Pekin *et al.*, Direct measurement of nanostructural change during in situ deformation of a bulk metallic glass. *Nat. Commun.* **10**, 1–7 (2019).
23. E. J. Frankberg *et al.*, Highly ductile amorphous oxide at room temperature and high strain rate. *Science* **366**, 864–869 (2019).
24. K. Qiu *et al.*, Self-healing of fractured diamond. *Nat. Mater.* **22**, 1317–1323 (2023).
25. L. W. Yang *et al.*, Mechanical properties of metal-ceramic nanolaminates: Effect of constraint and temperature. *Acta Mater.* **142**, 37–48 (2018).
26. J. Zhang *et al.*, Plastic deformation in silicon nitride ceramics via bond switching at coherent interfaces. *Science* **378**, 371–376 (2022).
27. S. Kondo, T. Mitsuma, N. Shibata, Y. Ikuhara, Direct observation of individual dislocation interaction processes with grain boundaries. *Sci. Adv.* **2**, 1–8 (2016).
28. D. Bufford, Y. Liu, J. Wang, H. Wang, X. Zhang, In situ nanoindentation study on plasticity and work hardening in aluminium with incoherent twin boundaries. *Nat. Commun.* **5**, 4864 (2014).
29. S. Kondo, A. Ishihara, E. Tochigi, N. Shibata, Y. Ikuhara, Direct observation of atomic-scale fracture path within ceramic grain boundary core. *Nat. Commun.* **10**, 1–6 (2019).
30. L. Feng, R. Hao, J. Lambros, S. J. Dillon, The influence of dopants and complexion transitions on grain boundary fracture in alumina. *Acta Mater.* **142**, 121–130 (2018).
31. J. W. Obreimoff, The splitting strength of mica. *Proc. R. Soc. Lond. A* **127**, 290–297 (1930).

Downloaded from https://www.pnas.org by "IMPERIAL COLLEGE LONDON, SUBSCRIPTIONS & E ACCESS" on October 22, 2024 from IP address 146.179.87.8.

32. A. Kelling *et al.*, Investigating fracture of nanoscale metal-ceramic multilayers in the transmission electron microscope. *Scr. Mater.* **115**, 42–45 (2016).
33. P. M. Kelly, C. J. Wauchope, The tetragonal to monoclinic martensitic transformation in zirconia. *Key Eng. Mater.* **153–154**, 97–124 (1998).
34. J. Rödel, J. F. Kelly, B. R. Lawn, In situ measurements of bridged crack interfaces in the scanning electron microscope. *J. Am. Ceram. Soc.* **73**, 3313–3318 (1990).
35. G. R. Irwin, *Fracture* (Springer-Verlag, Berlin, Germany, 1958), vol. 6.
36. D. Broek, *Elementary Engineering Fracture Mechanics* (Martinus Nijhoff Publishers, The Hague, Boston, MA, 1984).
37. K. Kishida, Y. Shinkai, H. Inui, Room temperature deformation of ^{6}H-SiC single crystals investigated by micropillar compression. *Acta Mater.* **187**, 19–28 (2020).
38. D. Wilson, Z. Zheng, F. P. E. Dunne, A microstructure-sensitive driving force for crack growth. *J. Mech. Phys. Solids* **121**, 147–174 (2018).
39. J. Chevalier, L. Gremillard, A. V. Virkar, D. R. Clarke, The tetragonal–monoclinic transformation in zirconia: Lessons learned and future trends. *J. Am. Ceram. Soc.* **92**, 1901–1920 (2009).
40. A. G. Evans, R. M. Cannon, Toughening of brittle solids by martensitic transformations. *Acta Metall.* **34**, 409–443 (1986).
41. R. P. Ingel, I. I. I. Lewis, David., Elastic anisotropy in zirconia single crystals. *J. Am. Ceram. Soc.* **71**, 265–271 (1988).
42. E. Camposilvan, M. Anglada, Size and plasticity effects in zirconia micropillars compression. *Acta Mater.* **103**, 882–892 (2016).
43. K. Yoshida *et al.*, Large increase in fracture resistance of stishovite with crack extension less than one micrometer. *Sci. Rep.* **5**, 1–2 (2015).
44. J. Eichler, M. Hoffman, U. Eisele, J. Rödel, R-curve behaviour of 2Y-TZP with submicron grain size. *J. Eur. Ceram. Soc.* **26**, 3575–3582 (2006).
45. R. H. J. Hannink, P. M. Kelly, B. C. Muddle, Transformation toughening in zirconia-containing ceramics. *J. Am. Ceram. Soc.* **83**, 461–487 (2000).
46. M. Hayakawa, N. Kuntani, M. Oka, Structural study on the tetragonal to monoclinic transformation in arc-melted ZrO_2-2mol.%Y_2O_3-I experimental observations. *Acta Metall.* **37**, 2223–2228 (1989).

Downloaded from https://www.pnas.org by "IMPERIAL COLLEGE LONDON, SUBSCRIPTIONS & E ACCESS" on October 22, 2024 from IP address 146.179.87.8.